Photoionization cross section and resonance structure of Cl I

Ellen R. Brown, Steven L. Carter, and Hugh P. Kelly
Department of Physics, University of Virginia, Charlottesville, Virginia 22901
(Received 23 July 1979)

The photoionization cross sections for the $3p$ and $3s$ subshells of the ground state of atomic chlorine have been calculated using many-body perturbation theory. We find significant electron-electron correlation effects for both cross sections. Resonances due to the $3p^4nd$, $3p^4ns$, and $3s3p^5np$ configurations, and relaxation effects in the $3p$ subshell cross sections were also calculated.

I. INTRODUCTION

Accurate calculations of the photoionization cross section for an atom test the atomic physicist's ability to identify and understand physically important correlation effects. Calculations have recently been carried out on open-shell systems, which theorists find particularly challenging, by using methods such as the many-body perturbation theory (MBPT) of Brueckner[1] and Goldstone,[2] the R matrix,[3-5] and the random-phase approximation with exchange (RPAE).[6,7]

In this paper we present results for the photoionization cross sections $\sigma(\omega)$ of the $3s$ and $3p$ subshells of neutral chlorine in an energy range extending from the $3p^4\,^3P$ threshold to 45 eV. At present the only experimental data are ratios of partial cross sections at one energy.[8] However, $\sigma(\omega)$ for chlorine is interesting because there have been several conflicting calculations[5-7,9] all of which include correlations. In addition, Hartree-Fock calculations have been reported.[10]

Our work is based on MBPT as applied to atoms[11] using LS-coupled states to separately calculate the cross section for each final LS-coupled channel.[12] Details of the theory are discussed in Sec. II, with emphasis on new features of the calculation. These include a coupled-integral-equations technique used to evaluate certain classes of electron-electron correlations to all orders.

In Sec. III we present numerical results for the total $\sigma(\omega)$ in both the resonant and nonresonant regions and for the $\sigma(\omega)$ of selected LS-coupled channels. Comparison is made with results of previous calculations. We also discuss relaxation effects and compare the ratios of our partial cross sections at 21.2 eV with recent experimental results.[8] Conclusions and a summary follow in Sec. IV.

II. THEORY

A. Perturbation expansion

We base our calculation on the electric dipole approximation; spin-orbit coupling and other relativistic effects are omitted. The prescription for $\sigma(\omega)$ is[13]

$$\sigma(\omega) = (4\pi/c)\omega\ \mathrm{Im}\alpha(\omega)\,, \tag{1}$$

where $\mathrm{Im}\alpha(\omega)$ is the imaginary part of the frequency-dependent dipole polarizability.[13] Atomic units are used throughout, except where otherwise noted.

The expansion for $\alpha(\omega)$ is developed for an atom described by the Hamiltonian

$$H = H_0 + H_c\,, \tag{2}$$

where

$$H_0 = \sum_{i=1}^{N}\left[-\tfrac{1}{2}\nabla_i^2 - (Z/r_i) + V(r_i)\right] \tag{3}$$

and

$$H_c = \sum_{i<j=1}^{N} v_{ij} - \sum_{i=1}^{N} V(r_i)\,. \tag{4}$$

The term v_{ij} represents the Coulomb interaction between pairs of electrons, and the single-particle potential $V(r_i)$ accounts for the average interaction of the ith electron with the remaining $N-1$ electrons.

In the dipole approximation there is a perturbing external electric field $F\hat{\mathbf{z}}\cos(\omega t)$ which adds the term

$$V_{\mathrm{ex}}(r,t) = F\cos\omega t \sum_{i=1}^{N} z_i \tag{5}$$

to H_c. This term leads to an expression for $\mathrm{Im}\alpha(\omega)$ in terms of dipole matrix elements. The dipole length matrix elements are expressed as

$$Z(p \to k) = \langle\psi_f|\sum_{i=1}^{N} z_i|\psi_0\rangle\,, \tag{6}$$

where ψ_0 and ψ_f are exact many-particle ground and excited (continuum) states, respectively, and ψ_f represents the excitation of the ground-state electron p to the excited state k. Dipole velocity matrix elements are formed when the right-hand side of Eq. (6) is replaced by

 © 1980 The American Physical Society

$$\frac{1}{E_0 - E_f}\left\langle \psi_f \left| \sum_{i=1}^{N} \frac{d}{dz_i} \right| \psi_0 \right\rangle. \tag{7}$$

Here E_0 and E_f are exact energy eigenvalues corresponding to ψ_0 and ψ_f, respectively. Continuum orbitals are normalized according to

$$P_k(r) = rR_k(r) = \cos[kr + (q/k)\ln(2kr) - \tfrac{1}{2}\pi(l-1) + \delta_l], \tag{8}$$

where $V(r) \to q/r$ as $r \to \infty$; the cross section then becomes

$$\sigma(\omega) = N''(8\pi\omega/ck)|Z(p \to k)|^2, \tag{9}$$

where N'' is a normalization correction[11] usually close to unity, $k = [2(\omega - I)]^{1/2}$, and I is the ionization energy.

Our basis set consists of linear combinations of determinants containing N different single-particle states which are solutions of

$$[-\tfrac{1}{2}\nabla^2 - (Z/r) + V(r)]\phi_n = \epsilon_n \phi_n. \tag{10}$$

The Russell-Saunders LSM_LM_S coupling scheme has been used throughout the calculation. Although we refer to the MBPT series of diagrams, it should be understood that the virtual and excited states are LS-coupled wave functions and that there is, in general, a different diagrammatic series for each LS-coupled channel.[12]

The matrix element $Z(p \to k)$ in Eq. (9) is evaluated by summing the series of open diagrams containing one dipole interaction and any number of perturbations of the form H_c.[14,15] Figure 1 illustrates typical terms in the perturbation expansion. Exchange interactions have always been included. The time ordering of the interactions proceeds from the bottom to the top of the diagrams, and the order of the correlation refers to the number of perturbations H_c. When the dipole interaction occurs first, the diagram contributes to the final-state correlations (FSC), as in Fig. 1(b), and has an energy denominator of the form

$$D = \sum_{i=1}^{N'} (\epsilon_{p_i} - \epsilon_{k_i}) + \omega, \tag{11}$$

where ϵ_{p_i} and ϵ_{k_i} are the single-particle energies of a hole-particle pair, and N' is the number of pairs excited. If the denominator in Eq. (11) vanishes, it is evaluated according to

$$\lim_{\eta \to 0}(D + i\eta)^{-1} = \mathrm{P}(D^{-1}) - i\pi\delta(D), \tag{12}$$

where P indicates principal-value integration. When the perturbation precedes the dipole interaction, the diagram contributes to the ground-state correlations (GSC), as in Fig. 1(c), and has an energy denominator of the form

$$D = \sum_{i=1}^{N'} (\epsilon_{p_i} - \epsilon_{k_i}). \tag{13}$$

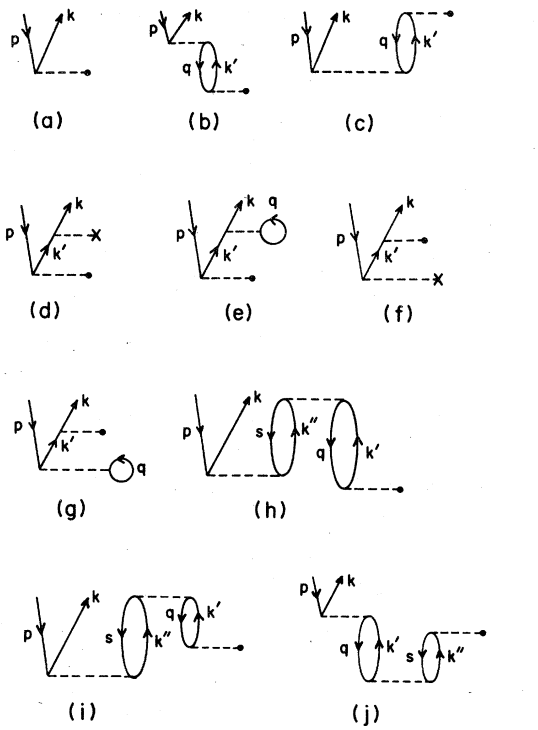

FIG. 1. Diagrams that contribute to the matrix element $Z(p \to k)$. Dashed line ending with isolated solid dot indicates matrix element of z. The cross indicates interaction with the potential $V(r)$. Other dashed lines represent Coulomb interactions. Exchange diagrams are also included.

Although our single-particle states were calculated in a Hartree-Fock (HF) V^{N-1} potential,[16] the diagrams of Figs. 1(b), 1(d), and 1(e) do not necessarily cancel one another (as they do in the closed-shell case[16]), even if p and q belong to the same subshell, and k and k' have the same orbital angular momentum. This happens because p and q may represent electrons which correspond to different ionic cores. These electrons are excited to different channels k and k', each with excited states calculated in V^{N-1} potentials corresponding the LS coupling of the channel. The diagrams of Figs. 1(b), 1(d), and 1(e) were evaluated by the coupled-integral-equations technique (described in Sec. IIC). Diagrams represented in Figs. 1(f) and 1(g) were evaluated by the differential-equation technique.[17] No normalization terms[11] were included in this calculation. In Ar they resulted in a 2.3% decrease in the final cross section,[18] and a similar small decrease can be expected in Cl.

We ensured orthogonality of the excited-state wave functions with the ground-state orbitals of the same angular momentum by including projection operators in the potential.[19] Typical values

TABLE I. Resonance configurations and the final channels in which they occur.

Resonant configuration	Final channels of occurrence
$^1Dns^2D$	$^3Pkd^2D$
$^1Dnd^2D$	$^3Pkd^2D$
$^1Dnd^2P$	$^3Pkd^2P$, $^3Pks^2P$
$^1Snd^2D$	$^1Dkd^2D$, $^1Dks^2D$, $^3Pkd^2D$
$^1Sns^2S$	$^1Dkd^2S$
$^3Pnp^2D$	$^3Pkd^2D$, $^1Dkd^2D$, $^1Skd^2D$, $^1Dks^2D$
$^3Pnp^2P$	$^3Pkd^2P$, $^1Dkd^2P$, $^3Pks^2P$
$^3Pnp^2S$	$^1Dkd^2S$, $^1Sks^2S$
$^1Pnp^2D$	$^3Pkd^2D$, $^1Dkd^2D$, $^1Skd^2D$, $^1Dks^2D$, $^3Pkp^2D$
$^1Pnp^2P$	$^3Pkd^2P$, $^1Dkd^2P$, $^3Pks^2P$, $^3Pkp^2P$
$^1Pnp^2S$	$^1Dkd^2S$, $^1Sks^2S$, $^3Pkp^2S$

for the overlap between the ground- and excited-state orbitals were 10^{-5} or better.

Throughout the calculation we used experimental $3s$ and $3p$ removal energies from Moore's tables.[20] Although the MBPT prescription calls for single-particle energies, by using the available experimental values at the outset we semiempirically include the summation of certain classes of diagrams which shift the single-particle energies towards their experimental values.[11]

B. Resonances

The energy denominator of a final-state correlation (FSC) diagram may vanish when the bound intermediate configuration is degenerate with the continuum. When this happens, the bound configuration contributes to resonances. Table I lists the resonant configurations which were included in this work.

In previous many-body calculations[12,18,21] the resonance structure has been evaluated by using one of two techniques. In the first, the isolated-resonance formulation,[13,18] each resonance is treated as though it were independent of all others in the series. Figures 2(a) and 2(b) are split at the virtual $q \rightarrow n$ state, and diagram segments such as those in Figs. 2(c) and 2(d) are inserted to form a geometric series. [The horizontal line in Figs. 2(b), 2(c), and 2(e) indicates an imaginary contribution.] In the second method,[12,13,21] an interacting resonance series is formed by adding diagram segments such as those in Fig. 2(e) to the top of the diagrams in Figs. 2(a) and 2(b).

Most of the resonance structure for Cl was calculated via the coupled-integral-equations technique (described below). The isolated-resonance technique was used for cases where the interchannel coupling was estimated to be weak and where there was sufficient separation in energy from other resonant series that one would expect little interaction between them.

C. Coupled integral equations

The ^2P ground state of Cl has a $3s^23p^5$ configuration. When a $3p$ electron is photoionized ($3p \rightarrow kd$ or $3p \rightarrow ks$), three core couplings ($^1S, ^1D, ^3P$) and three final couplings ($^2S, ^2P, ^2D$) combine to give nine possible channels. For each of these nine channels sets of excited-state bound and continuum orbitals were calculated in the unique V^{N-1} potential[11] appropriate to the LS coupling of the channel. If one then evaluates a first-order FSC diagram such as Fig. 1(b), where p and q refer to the same ionic cores, and k and k' represent states calculated in the same potential, the two-electron (Coulomb) interactions are cancelled by interactions with the potential.[16] (We refer to these FSC diagrams as being diagonal.) However, when p and q in Fig. 1(b) refer to different ionic cores, and states k and k' have the same angular momenta,

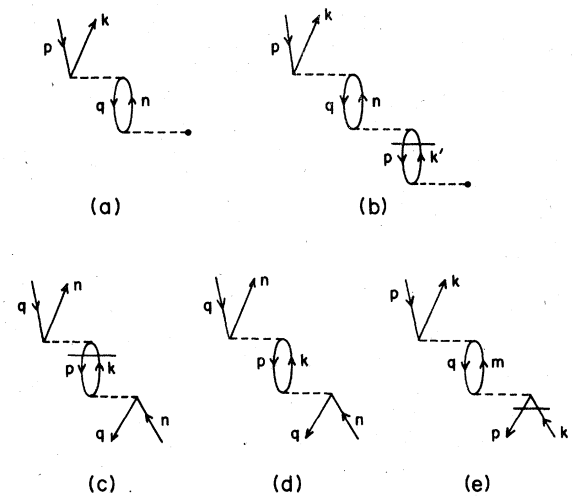

FIG. 2. Diagrams and diagram segments associated with resonances. Horizontal line indicates that the denominator should be treated according to $-i\pi\delta(D)$.

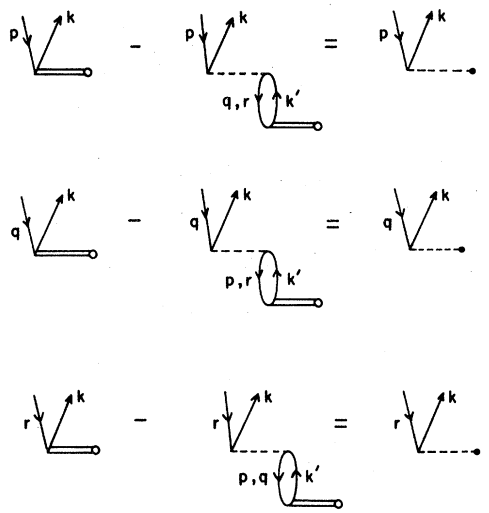

FIG. 3. Symbolic representation of the coupled equations for three-channel coupling. The double bar line represents the correlated dipole matrix element.

the interaction with the potential vanishes. The remaining Fig. 1(b) contributions (we refer to these FSC diagrams as being nondiagonal) can be comparable in magnitude to the contributions from the lowest-order dipole matrix elements corresponding to each outgoing channel. Therefore to improve accuracy of the perturbation expansion, the effects of these nondiagonal terms are calculated to infinite order. Core states appropriate to a given final coupling are mixed by solving a set of coupled integral equations for the unknown correlated dipole matrix elements corresponding to each core.

The coupled equations are shown schematically in Fig. 3 for the case of three-channel coupling. The first line of Fig. 3 represents the equation

$$\overline{D}_p(k) - \sum_{s\neq p}\sum_{k'} \frac{V_{p,s}(k,k')\overline{D}_s(k')}{\epsilon_s - \epsilon_{k'} + \omega} = D_p(k)\,, \qquad (14)$$

where $\overline{D}_s$ (D_s) is the correlated (uncorrelated) dipole matrix element for channel s, and $V_{p,s}$ is the correlation-interaction (Coulomb) matrix element between channels p and s. The sum over high-lying intermediate bound states, usually accounted for with the n^{-3} rule,[11] is handled in Eq. (14) by a back-extrapolation of the continuum matrix elements into the region between the last explicitly calculated bound state and $k'=0$. By then making discrete the integral over intermediate continuum states k', the coupled equations of Fig. 3 become a matrix equation easily solved by standard techniques. As applied to Cl, the labels p, q, and r of Fig. 3 could represent, for example, the three channels $^1D\,kd\,^2D$, $^3P\,kd\,^2D$, and $^1S\,kd\,^2D$. Any number of channels can be coupled but only if the total L and S is the same in all cases. We note that the coupled equations of Fig. 3 actually solve for the K matrix.[13,22] This procedure is also equivalent to that of a close-coupling calculation on the continuum orbitals.[23]

In practice, the lowest-order dipole matrix elements were replaced by "effective lowest-order" dipole matrix elements, consisting of the sum of the lowest-order dipole matrix elements and all first-order GSC diagrams as shown in Figs. 1(a) and 1(c). These results then differ from a K matrix or close-coupling calculation by including ground-state correlations. This change enables one to include terms from Fig. 1(j) and was found to bring the length and velocity cross sections a few percent closer than they were when these terms were included perturbatively. The sum of Figs. 1(h) and 1(i) when k and k' represent different sets of kd states was included in the coupled-equations program by adding the appropriate Coulomb matrix elements to the first-order Coulomb matrix elements indicated in Fig. 3. The portions of Figs. 1(h) and 1(i) for which k and k' represent the same sets of kd states were evaluated later, using fully correlated dipole matrix elements generated from the code.

III. RESULTS

A. $3p \rightarrow kd$, ks channels

Cross sections for each of the $3p \rightarrow kd$ channels were calculated twice, first using frozen-core orbitals (of the neutral atom) which excluded relaxation effects, then approximating these effects by calculating the excited-state orbitals in the field of fully self-consistent ionic-core orbitals (^1S, ^1D, ^3P couplings). In Fig. 4 we have labeled our lowest-order HF $3p \rightarrow kd, ks$ $\sigma(\omega)$ curves which

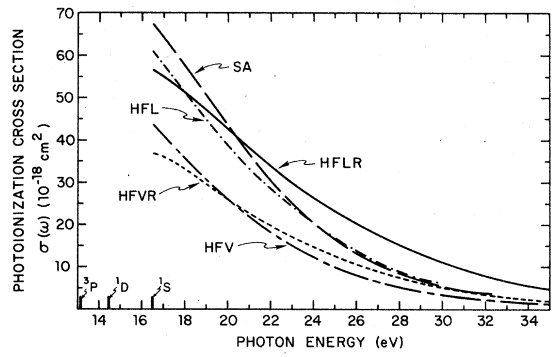

FIG. 4. Total $3p \rightarrow kd$, ks lowest-order HF $\sigma(\omega)$ vs photon energy past the ^1S edge. HFLR (HFVR) indicates length (velocity) form of $\sigma(\omega)$ when relaxation effects are included. HFL (HFV) indicates length (velocity) form of $\sigma(\omega)$ when relaxation effects are not included. SA indicates the Starace and Armstrong (Ref. 6) RPAE $\sigma(\omega)$.

TABLE II. Percent difference between length and velocity cross sections including correlations [a] for the $kd\,^2P$, ^2D channels at 16.62 eV (near the ^1S edge).

Channel	Unrelaxed difference [b] (%)	Relaxed difference [b] (%)
$^3P\,kd\,^2P$	14	22
$^1D\,kd\,^2D$	6	11
$^1S\,kd\,^2D$	26	26
$^1D\,kd\,^2P$	22	23
$^3P\,kd\,^2D$	9	8

[a] Includes correlations from coupled-equations method.
[b] In all cases length results are greater than velocity.

include relaxation effects HFLR (length), and HFVR (velocity); our $\sigma(\omega)$ curves which exclude these effects are labeled HFL (length) and HFV (velocity). In Fig. 4 we compare these results to those of Starace and Armstrong[6] (labeled SA) in the region past the ^1S edge. Our frozen-core HF results indicate that at the ^1S edge the $^3P\,kd\,^2D$ channel contributes approximately 34% of the total cross section as compared to $^1D\,kd\,^2P$ (16%), $^3P\,kd\,^2P$ (13%), $^1D\,kd\,^2S$ (8%), $^1D\,kd\,^2D$ (12%), and $^1S\,kd\,^2D$ (11%). (After relaxation effects are included the percent contribution of the individual channels changes by less than 2%, but the HFL is decreased by 7% and the HFV curve by 15%.) In this energy range the $3p \rightarrow ks$ channels contribute a total of less than 3 Mb or 6% of the total $\sigma(\omega)$. Our values for the contributions from each individual $3p \rightarrow kd, ks$ channel are similar to the HF values presented in Tables II–IV of Starace and Armstrong.[6] In the frozen-core approximation, the lowest-order Cooper minima[13] for the $^3P\,kd$ channels occur at about 46 eV, for the $^1D\,kd$ channels at about 41 eV, and for the $^1S\,ks$ channel at about 37 eV. The minima were within about 5 eV of those values when relaxation effects were included.

In the kd channels, the largest diagrams are of the form of Fig. 1(b), where p and q correspond to different ionic cores and where the intermediate and final excited states have the same angular momenta ($l=2$) but are calculated in potentials corresponding to the different ionic cores (nondiagonal contributions). We include these important diagrams to infinite order using the coupled-integral-equations technique explained in Sec. IIC, in which we also include the nondiagonal portions of Figs. 1(h) and 1(i) (where p and q refer to different ionic cores) for all six kd channels. [The remaining portions of Figs. 1(h) and 1(i) were included separately.] Figures 1(h) and 1(i) were evaluated for $s=3p$, $k''=k''d$, $q=3p$, and $k'=k'd$, and also for $s=3s$, $k''=3p$, $q=3p$, and $k'=k'd$.

The geometric means[24] of our final length and velocity results (relaxed and unrelaxed) for the five individual ^2P and ^2D channels past the ^1S edge are presented in Figs. 5 and 6. Table II shows the percent difference between the length and velocity cross sections for all $kd\,^2P$, ^2D channels near the ^1S edge.

There is only one $kd\,^2S$ channel, namely $^1D\,kd\,^2S$.

TABLE III. Sum of the $3p \rightarrow kd, ks$ cross sections at various energies (in 10^{-18} cm^2).

	With relaxation effects				Without relaxation effects			
Photon	Lowest-order HF		Correlated [a]		Lowest-order HF		Correlated [a]	
energy (eV)	Length	Velocity	Length	Velocity	Length	Velocity	Length	Velocity
16.62	56.14	37.05	35.91	34.00	60.40	43.06	39.40	35.99
18	51.66	33.30	36.13	34.71	51.10	35.60	40.10	36.36
20	42.60	26.41	35.38	31.62	38.79	25.92	39.38	35.49
21.2	37.22	22.46	34.32	30.10	32.48	21.11	37.81	34.02
23	29.98	17.32	32.06	29.57	24.33	15.17	33.94	30.55
25	23.17	12.71	28.45	23.34	16.97	10.13	27.52	24.87
27	17.51	9.11	24.17	21.46	11.31	6.49	20.33	18.38
30	11.03	5.30	17.40	12.89	5.87	3.18	11.52	10.37
32	7.75	3.54	13.01	10.94	3.64	1.95	7.17	6.44
35	4.45	1.89	7.87	5.16	1.69	0.92	3.19	2.85
40	1.61	0.70	2.83	2.19	0.68	0.50	0.93	0.85
45	0.57	0.36	0.88	0.68	0.42	0.45	0.38	0.38

[a] Includes correlations from coupled-equations method.

TABLE IV. Ratios of partial cross sections for Cl at 21.2 eV.

Final state [a]	With relaxation [b]	Without relaxation [b]	Starace-Armstrong [c]	Geometric ratio [d]	Geometric ratio [e]	Experiment [f]
^3P	1.500 (1.500)	1.500 (1.500)	1.50	1.500	1.500	1.50
^1D length	0.743 (0.702)	0.685 (0.453)	0.57			
^1D velocity	0.790 (0.834)	0.718 (0.585)		0.833	0.802	0.81
^1S length	0.128 (0.176)	0.106 (0.109)	0.18			
^1S velocity	0.144 (0.195)	0.124 (0.132)		0.167	0.159	0.16

[a] Multiplet of $Cl^+(3p)^4$.
[b] Includes correlations from coupled-equations method. Lowest-order result in parentheses.
[c] RPAE calculation by Starace and Armstrong, Ref. 6.
[d] Simple geometric ratio.
[e] Improved geometric ratio, Berkowitz and Goodman, Ref. 32.
[f] Photoelectron experiment by Kimura *et al.*, Ref. 8.

Hence, Fig. 1(b) with $p,q = 3p$ and $k,k' = {}^1D\ kd\,{}^2S$ and its exchanges cancels with Figs. 1(d) and 1(e). The $3s3p^6\,{}^2S$ intermediate state contributes only to correlations in the $^1D\ kd\,{}^2S$ channel; the dominant first-order correlation in the $^1D\ kd\,{}^2S$ channel is Fig. 1(b) with $q = 3s$ and $k' = 3p$. When this correction is evaluated with the energy level of the $3s3p^6$ state taken to be the Cowan and Radziemski[25] value of −0.309 378 a.u., it has the same sign as the lowest-order dipole matrix element and is slightly larger in magnitude. Figure 1(b) is responsible for the huge change shown in Fig. 7 between the geometric mean[24] of the length and velocity forms of the lowest-order HF $\sigma(\omega)$ for this channel (labeled GHF and GHFR for unrelaxed and relaxed, respectively) and the $\sigma(\omega)$ including first-order corrections (labeled GF).

Since the $3s \rightarrow 3p$ correction is so important, the coupled equations were used to correlate the $3p \rightarrow {}^1D\ kd\,{}^2S$ and $3s \rightarrow 3p$ dipole matrix elements to infinite order, which resulted in a shift of the HF curve by approximately 7.5 eV to the right. Based on the Cowan and Radziemski[25] calculation, we made an approximation of the energy shifts not included by the coupled-equations technique. The correction amounts to −0.022 901 a.u. and was added to the ΔE_{SCF}, $E_{HF}\ 3s^2 3p^5 - E_{HF} 3s3p^6$, to obtain the energy actually used in the calculation.

The geometric mean[24] of the length and velocity results of our total $\sigma(\omega)$ for the $^1D\ kd\,{}^2S$ channel is also shown in Fig. 7 for both the relaxed (GTR) and unrelaxed (GT) calculations. The dipole length and velocity results for each set of curves presented in Fig. 7 differ by less than 25% at the ^1D

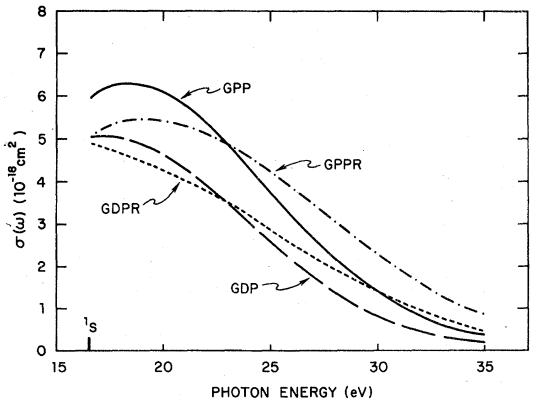

FIG. 5. Geometric mean of the length and velocity forms of our most fully correlated individual $kd\,{}^2P$ cross sections vs photon energy past the ^1S edge. GPPR (GDPR) indicates relaxation effects are included in the $^3P\ kd\,{}^2P$ ($^1D kd\,{}^2P$) channel calculations. GPP (GDP) indicates relaxation effects are not included in the $^3P\ kd\,{}^2P$ ($^1D kd\,{}^2P$) channel calculations.

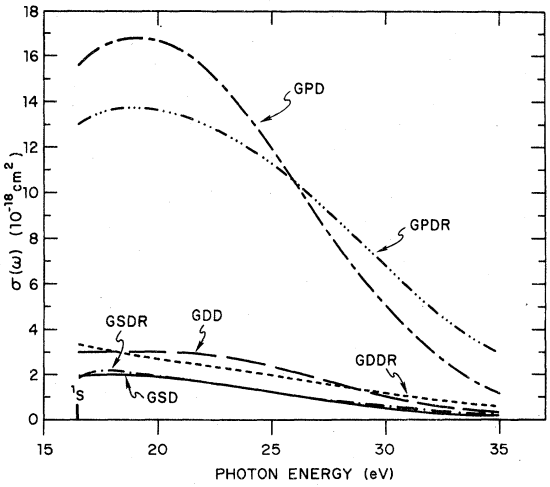

FIG. 6. Geometric mean of the length and velocity forms of our most fully correlated $kd\,{}^2D$ cross sections vs photon energy past the ^1S edge. GPDR, GDDR, and GSDR indicate relaxation effects are included in the $^3P\ dk\,{}^2D$, $^1D kd\,{}^2D$, and $^1S kd\,{}^2D$ channels, respectively. GPD, GDD, and GSD indicate relaxation effects are not included in the $^3P\ kd\,{}^2D$, $^1D kd\,{}^2D$, and $^1S kd\,{}^2D$ channels, respectively.

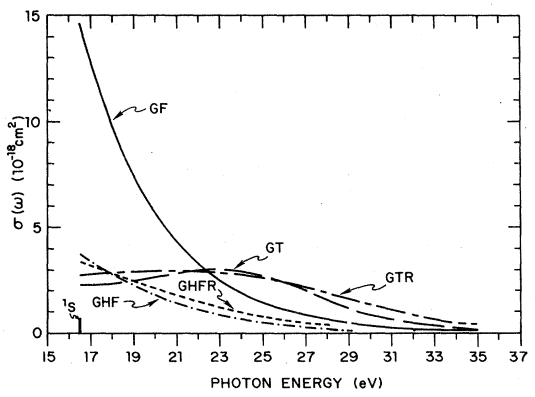

FIG. 7. Geometric mean of the length and velocity forms of $\sigma(\omega)$ vs photon energy for the $^1Dkd\,^2S$ channel. GHRF (GHF) represent HF values when relaxation effects are (are not) included. GTR (GT), represent our most fully correlated values for $\sigma(\omega)$ when relaxation effects are (are not) included. GF represents the $\sigma(\omega)$ after first-order corrections have been included (relaxation effects not included).

edge. Since the ks channels contributed so little to the total $\sigma(\omega)$, only first-order corrections were included and only frozen-core ks states were calculated.

Figure 8 compares the length and velocity forms of the total $3p \rightarrow ks, kd$ cross sections in

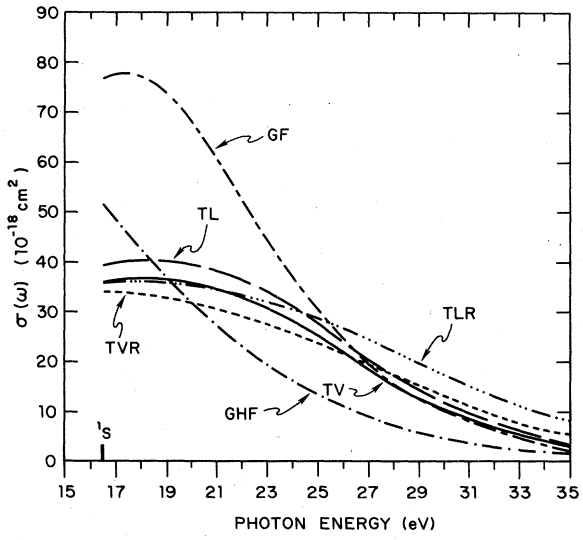

FIG. 8. Length and velocity forms of the sum of our final $3p \rightarrow kd, ks$ cross sections when relaxation effects are included (TLR, TVR, respectively) and when they are not included (TL, TV), respectively). Geometric mean of the length and velocity forms of the sum of the $3p \rightarrow kd, ks$ cross sections are shown for the unrelaxed lowest-order Hartree-Fock calculation (GHF) and after first-order corrections have been included (GF). Resonance structure is not included in this figure, but is presented in subsequent figures.

both the relaxed and unrelaxed forms. Figure 8 also shows the geometric mean[24] of the length and velocity forms of $\sigma(\omega)$ for the HF calculation and of $\sigma(\omega)$ after the first-order corrections were evaluated. Near the ^1S edge the final unrelaxed results show a decrease in $\sigma(\omega)$ by approximately 35% from the lowest order (HF) values and by approximately 50% from the first-order values. Beyond 26 eV, the total results (excluding relaxation effects) for $\sigma(\omega)$ tail into the first-order values; the total $\sigma(\omega)$ when relaxation effects are included are considerably higher than our other results in this energy range.

When photon energies are relatively low, the kinetic energy of the photonionized electron is correspondingly low and the photoionization process takes longer than it does at higher photon energies. Hence, at low photon energies the atom has time to rearrange (relax), and one would expect the relaxed calculation to be more accurate than the unrelaxed. At high photon energies the unrelaxed calculation is expected to be the more accurate. Table III gives the values of our lowest-order HF and total cross sections for both the relaxed and unrelaxed cases.

B. $3s \rightarrow kp, kf$ channels

The sum of the lowest-order (unrelaxed) HF cross sections for the six $3s \rightarrow kp$ channels is presented in Fig. 9 along with the sum of these cross sections obtained when correlations are included. First-order GSC diagrams were evaluated, and ω-dependent (correlated) $3p \rightarrow kd$ and $3s \rightarrow 3p$ dipole matrix elements were used to evaluate the diagrams of Figs. 1(b), 1(h), and 1(i). All other first-order FSC diagrams were evaluated with lowest-

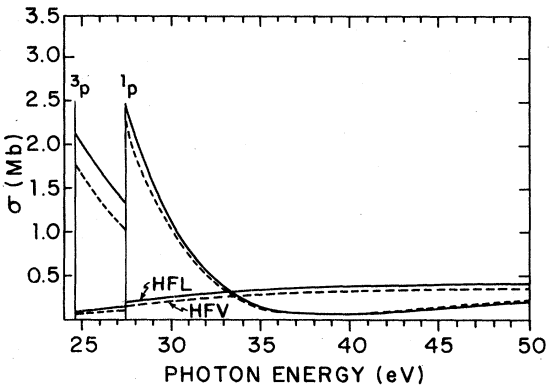

FIG. 9. Correlated $\sigma(\omega)$ vs photon energy for the sum of the $3s \rightarrow kp$ transitions. Solid line is length calculation, dashed is velocity. Lowest-order values are labeled HFL and HFV and are shown for comparison. Resonance structure is not included in this figure, but is presented in subsequent figures.

order dipole matrix elements.

A comparison between our correlated $3s \rightarrow kp$ $\sigma(\omega)$ and the HF result is similar to that[26-28] in Ar, where correlations produced a sharp increase in $\sigma(\omega)$ at threshold, in good agreement with experiment.[29] The total $\sigma(\omega)$ for the kp channels dips to a minimum at about 39 eV, an energy in the same range as the Cooper minimum[13] in the $3p \rightarrow kd$ dipole matrix elements. Length and velocity agree to within 2% in the $^1P\,kp$ channels near the ^1P edge, and to within 10% in the $^3P\,kp$ channels near the ^3P edge.

In the dipole approximation there is no lowest-order contribution to the $3s \rightarrow kf$ cross section. However, when first-order correlations are included, contributions to the $3s \rightarrow kf$ cross section exist. The first-order correlations were evaluated and were found to contribute approximately 10^{-3} Mb. Figures 1(b) and 1(g) where $q = 3p$ and $k' = kd\,^2D$ were sizable, but tended to cancel one another. The analogous $3p \rightarrow kg$ cross section is estimated to be very small and has therefore been neglected.

C. Total nonresonant cross section

Our length and velocity results for the total $\sigma(\omega)$, the sum of the $3p \rightarrow kd, ks$ (excluding relaxation effects) and $3s \rightarrow kp, kf$ subcross sections, are shown in Fig. 10, where they are compared with other calculations. Resonance structure has been omitted. At the ^1S edge our length and velocity results agree to within 12%, and represent about a 41% decrease in the length form from the lowest-order HF values. The decrease is due to strong coupling between core states appropriate to a given final coupling (e.g., $^3P, ^1D, ^1S$ for ^2D).

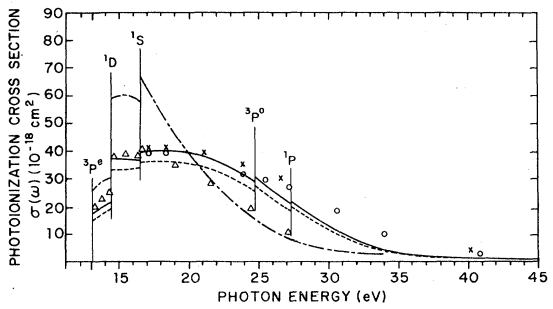

FIG. 10. Sum of $3s$ and $3p$ (unrelaxed) subshell photoionization cross sections vs photon energy for Cl I. The ^3P and ^1P edges near 25 eV are due to $3s$ photoionization. Solid (dashed) curve represents dipole length (velocity) matrix elements; dash-dot curve is from the calculation by Starace and Armstrong (Ref.6); open circles: Lamoureux and Combet Farnoux (Ref. 5) (length); cross marks: Conneely (Ref. 9) (length); triangles: Cherepkov and Chernysheva (Ref. 7). Resonance structure is not included in this figure, but is presented in subsequent figures.

The open-shell RPAE calculation of Cherepkov and Chernysheva[7] differs from that of Starace and Armstrong[6] between the ^1S threshold and about 22 eV. The RPAE calculation of Starace and Armstrong[6] omitted coupling between final ionic cores, and we believe that this accounts for the disagreement with the other calculations. Beyond 22 eV the two RPAE calculations[6,7] are in close agreement and lower than the present calculation. The R-matrix calculation of Lamoreux and Combet Farnoux[5] and the close-coupling calculation of Conneely[9] are in good agreement with each other and somewhat higher than the present calculation at high energies. Near the ^1S edge our results are in close agreement with the length calculation of Conneely.[9] However, his velocity calculation[9] (not shown) is almost a factor of 2 lower. Preliminary work by Armstrong[30] using a multiconfiguration calculation[31] and the K matrix to couple the different outgoing channels shows very promising results and excellent agreement between length and velocity.

Kimura *et al.*[8] have measured the ratios of the ^1D and ^1S cross sections to the ^3P cross section at an energy of 21.2 eV. A comparison between their values and our results is given in Table IV. We also include the RPAE results of Starace and Armstrong,[6] and the geometric ratio of Berkowitz and Goodman[32] in this table.

It was pointed out to us by Berkowitz[33] that the ratio of the ^1D and ^1S cross sections to the ^3P cross section could be predicted very accurately for Cl and also quite well for Br and I by means of an intermediate-coupling angular momentum treatment combined with spectroscopic mixing parameters. These results are shown in the sixth column of Table IV. Stimulated by the success of the calculation by Berkowitz and Goodman,[32] we calculated these ratios by simply evaluating the squares of the angular factors of the dipole matrix elements of Eq. (6) using LS coupling. Our geometric ratios are shown in the fifth column of Table IV and are in good agreement with the experimental ratios, although not as good as the ratios of Berkowitz and Goodman.[32] We justify the use of the angular dipole factors to estimate the ratios of cross sections by noting that although $\sigma(\omega)$ is inversely proportional to k as shown in Eq. (9), $Z(p \rightarrow k)$ is proportional to $k^{1/2}$ for small k so the dependence on k can be neglected to a first approximation.

Although the ratios of the ^1D and ^1S cross sections to the ^3P are given remarkably well by these geometric ratios, it is difficult to see how they can be used to predict total cross sections over a wide range of energies. For example, if we take

TABLE V. Ratios of the ^1D and ^1S cross sections to ^3P at various energies.[a]

Photon energy (eV)	With relaxation effects				Without relaxation effects			
	Lowest-order HF		Correlated[b]		Lowest-order HF		Correlated[b]	
	Length	Velocity	Length	Velocity	Length	Velocity	Length	Velocity
				^1D ratio[a]				
18	0.82	0.97	0.66	0.69	1.1	1.2	0.79	0.85
19	0.67	0.82	0.66	0.68	0.95	1.1	0.77	0.82
20	0.55	0.70	0.67	0.70	0.83	0.96	0.75	0.80
21.2	0.45	0.58	0.68	0.72	0.70	0.83	0.74	0.79
22	0.40	0.53	0.70	0.74	0.63	0.76	0.74	0.79
23	0.35	0.47	0.72	0.76	0.55	0.68	0.74	0.78
				^1S ratio[a]				
18	0.24	0.25	0.11	0.14	0.32	0.31	0.15	0.18
19	0.18	0.20	0.11	0.13	0.27	0.28	0.14	0.16
20	0.14	0.16	0.11	0.13	0.22	0.24	0.14	0.16
21.2	0.11	0.13	0.11	0.12	0.18	0.20	0.13	0.14
22	0.09	0.12	0.11	0.12	0.15	0.17	0.12	0.14
23	0.08	0.10	0.11	0.12	0.13	0.15	0.12	0.13

[a]Ratios shown are 1.5 times true ratio. This normalization is chosen to agree with that of Berkowitz and Goodman, Ref. 32.

[b]Includes correlations from coupled-equations method.

the Hartree-Fock result for the ^3P cross section and use the ratios to predict ^1D and ^1S, we obtain results that differ noticeably from our higher-order results, which we believe to be accurate to approximately 10–15%. Since we are considering ratios of cross sections, we note that the geometric estimate indicates that these ratios should be ω independent. Our lowest-order ratios indicated a rather large variation as a function of energy, whereas our final results showed considerably more stability (see Table V). We conclude that geometric ratios can only be used to calculate the total cross sections if one starts with a well-correlated ^3P cross section.

D. Resonant regions

The resonant series listed in Table I were calculated with either the coupled-equations or the isolated-resonance technique. Specific methods used for each series will be discussed since it is important to understand how the correlations were included in each channel. Frozen-core excited-state orbitals were used throughout the resonance calculations. All diagrams included in the nonresonant regions were also included in the resonant regions; if these diagrams were not explictly included in the codes used to generate the resonances, they were added to the resonant results before $\sigma(\omega)$ was evaluated. We consistently used calculated rather than experimental bound energies since not all of the latter are available. In Figs. 11–14 only the first four resonances in each series are explicitly shown, although each series extends to $n=\infty$.

Our current coupled-equations code is limited to coupling a maximum of four channels. Two considerations determined our choice of channels to be coupled during a single execution of the code: We tried to include those channels which are expected to interact most strongly, and we tried to maximize the amount of resonance information.

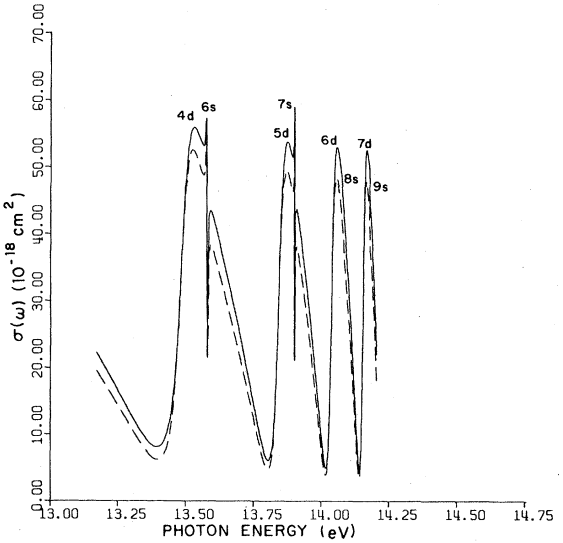

FIG. 11. The sum of the ^1Dnd and ns resonances in the ^2D and ^2P channels of Cl I. Resonances were truncated at 60 Mb. Solid (dashed) curve indicates dipole length (velocity) calculation. The narrow 8s and 9s resonances are not well resolved in this figure.

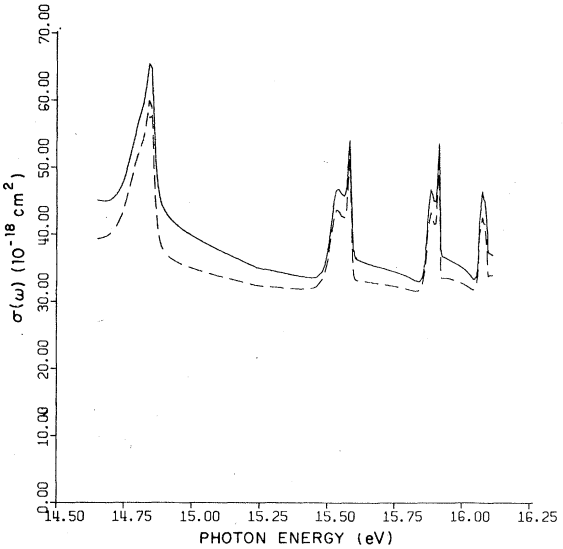

FIG. 12. $^1S\,nd$ and ns resonances in the ^2D channels and ^2S channels summed with the nonresonant ^2P channels of Cl*I*. Solid (dashed) curve indicates dipole length (velocity) calculation.

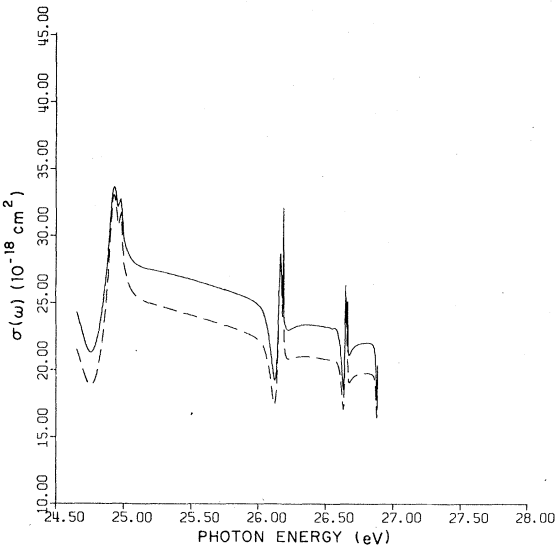

FIG. 14. $^1P\,np$ resonances in the ^2D, ^2P, ^2S channels. Solid (dashed) curve indicates dipole length (velocity) calculation.

Insofar as possible, we order the following discussion around the information generated from each set of input to the coupled-equations code.

We used the coupled-equations code with the three $kd\,^2D$ channels coupled with the $^1D\,ks^2D$ channel to generate the sum of the $^1D\,ns^2D$ and $^1D\,nd^2D$ resonances in the $^3P\,kd^2D$ channel. The $^1D\,nd^2P$ resonances in the $^3P\,kd^2P$ channel were calculated by coupling the two kd^2P channels.

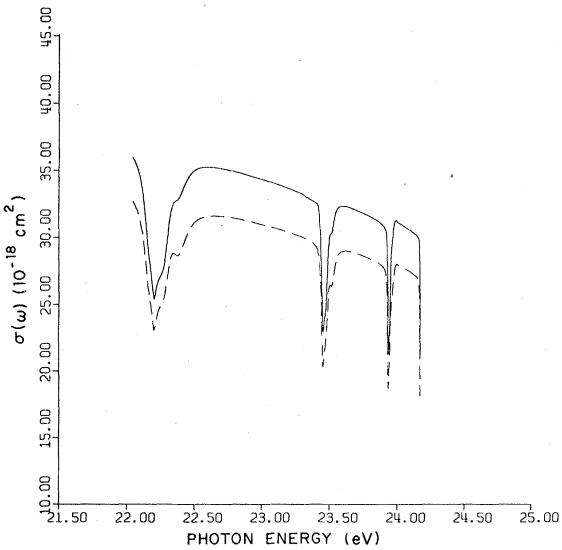

FIG. 13. $^3P\,np$ resonances in the ^2D, ^2P, and ^2S channels. Solid (dashed) curve indicates dipole length (velocity) calculation.

This same set of resonances in the $^3P\,ks^2P$ channel was similarly calculated by coupling the three kd, ks^2P channels. The sum of the $^1D\,nd, ns$ resonances in all of the $^2P, ^2D$ channels is presented in Fig. 11. We note that the ns resonances are very narrow and poorly resolved for the $8s$ and $9s$ cases shown.

The coupling of the three $kd\,^2D$ channels with the $^1D\,ks^2D$ was also used to calculate the $^1S\,nd\,^2D$ resonances for each channel in which they occur. Besides our results, the calculation by Lamoureux and Combet Farnoux[5] is the only other to show the first few resonances in the $^1S\,nd\,^2D$ series. The resonance structure in Ref. 5 was computed twice (calculations I and II) to show the effects of adding additional pseudo-orbitals. The $3d$ resonance in calculation I (II) is shifted approximately 0.1 eV (0.21 eV) to the right of ours and is wider than (approximately the same width as) ours. In both calculations of Ref. 5 the resonance is stronger than the one we calculate. The only other resonances presented by Lamoureux and Combet Farnoux[5] are from the $^1D\,nd\,^2P$ series, but they are not shown for low values of n.

The $^1S\,ns\,^2S$ resonances in the $^1D\,kd\,^2S$ channel were calculated by using the coupled equations to mix $^1D\,kd\,^2S$, $^3P\,kp^2S$, $^1S\,ks^2S$, and $3s3p^6\,^2S$. Figure 12 shows the sum of the $^1S\,ns^2S$ and $^1S\,nd\,^2D$ resonances in their respective ^2S and ^2D channels with the nonresonant background provided by the ^2P channels. The four ^2S states were also coupled to generate the $3s3p^5$, $^3P\,np^2S$ resonances in the $^1S\,ks^2S$ channel. We mixed $^1D\,kd\,^2S$, $^1P\,kp^2S$, $^3P\,kp^2S$, and $3s3p^6\,^2S$ to calculate the $^3P\,np\,^2S$ and

$^1Pnp^2S$ resonances in the $^1D\,kd^2S$ channel and the $^1Pnp^2S$ resonances in the $^3P\,kp^2S$ channel.

The $^3Pnp^2P$ ($^1Pnp^2P$) resonances were calculated in the $^3P\,kd^2P$ and $^1D\,kd^2P$ channels, again using the coupled equations for the three channels involved. All other resonant series listed in Table I were calculated by the isolated-resonance technique. Figure 13 shows the sum of the first four ^3Pnp resonances in the ^2D, ^2P, and ^2S channels, and Fig. 14 shows the sum of the first four ^1Pnp resonances in the ^2D, ^2P, and ^2S channels.

IV. SUMMARY AND CONCLUSIONS

We have presented the $3p \rightarrow kd, ks$ and $3s \rightarrow kp, kf$ cross sections of chlorine, including correlations, and have compared them with other calculations. We find that the perturbations which arise from configuration interaction between singly excited states of the same angular momentum but different ionic states of $Cl^+(3p^4)$ are large. When these corrections are evaluated to higher orders, they form a series which converges slowly. The series is summed by solving coupled integral equations which correspond to calculating the K matrix for an open-shell system. Our unrelaxed results in the region just beyond the ^1S edge are in good agreement with the RPAE calculation by Cherepkov and Chernysheva[7] and with the R-matrix calculation by Lamoureux and Combet Farnoux.[5]

We calculated the effects of relaxation, which appear to reduce the cross section by approximately 13% near the ^1S edge. At photon energies higher than 22 eV our cross section is somewhat larger than the RPAE results[7] and is in good agreement with the R-matrix calculation.[5] At photon energies beyond the onset of $3s \rightarrow kp$ photoionization, our cross section is lower than the R-matrix[5] and close-coupling[9] results, but higher than the RPAE[7] results.

We estimated relaxation effects in the $3p \rightarrow kd$ cross section by calculating excited states in the presence of $3p^4(^3P, ^1D, ^1S)$ states of Cl^+. We found that relaxation effects lowered the cross section near the ^1S edge but increased the cross section at high photon energies. One expects that our relaxed results will be less accurate than our unrelaxed results at higher energies. It would be desirable, but more difficult, to include relaxation effects by evaluating the appropriate diagrams. We plan to carry out such calculations in the future.

The ratios of the ^1D and ^1S cross sections at 21.2 eV to the ^3P value at that energy were evaluated, along with a simple geometric estimate of the ratios based on angular factors. We compare all of these results to the experimental work of Kimura *et al.*[8] and to the more complete geometric results of Berkowitz and Goodman,[32] who have obtained the best agreement with experiment. Whereas our unrelaxed lowest-order results disagree significantly with experiment, we find that our relaxed lowest-order length and velocity results straddle experiment and that our simple geometric ratios are very close to experimental values. The geometric mean of our ratios in both the correlated relaxed and unrelaxed calculations is lower than experiment.

The $3s3p^6\,^2S$ intermediate state is the dominant correlation to the $^1D\,kd^2S$ channel. Although one might expect the correction involving this intermediate state to produce a large change in the cross section, we find that after using the coupled equations to correlate the $3p \rightarrow {}^1D\,kd^2S$ and $3s \rightarrow 3p$ matrix elements the resulting cross section is similar in form to the lowest-order HF value, but shifted approximately 7.5 eV to the right.

We calculated the $3s \rightarrow kp$ cross sections, including correlations. The $3p \rightarrow kd$ correlations increased the value of the cross section near the $3s3p^5\,^{1,3}P$ thresholds by approximately an order of magnitude over the lowest-order HF value. This qualitative change in the behavior of the cross section is similar to the change noted in the calculations on argon, where the correlated results are in good agreement with experiment.

The first few resonances in each of the $3p \rightarrow nd, ns$ and $3s \rightarrow np$ series were evaluated and comparison was made between our $^1D\,nd^2S$ resonance-structure calculation and that of Lamoureux and Combet Farnoux.[5]

We find that correlation effects are significant in chlorine, and that in open-shell atoms it will often be necessary to consider final-state correlation effects which couple the various ionic cores.

ACKNOWLEDGMENTS

We wish to thank Dr. Charlotte Froese Fischer for the use of her Hartree-Fock code. We would also like to thank Dr. Knut Faegri, Jr. for programming aid and advice, Dr. M. Lamoureux and Dr. F. Combet Farnoux for providing us with a preprint of their work, Professor L. Armstrong and Dr. J. Berkowitz for helpful discussions, and Dr. Berkowitz for sending us a preprint of his work. This work was supported by the National Science Foundation, Grant No. PHY 7P-07154.

[1]K. A. Brueckner, Phys. Rev. 97, 1353 (1955); *The Many-Body Problem* (Wiley, New York, 1959).
[2]J. Goldstone, Proc. R. Soc. A 239, 267 (1957).
[3]M. LeDourneuf, V. K. Lan, P. G. Burke, and K. T. Taylor, J. Phys. B 8, 2640 (1975).
[4]P. G. Burke and K. T. Taylor, J. Phys. B 8, 2620 (1975).
[5]M. Lamoureux and F. Combet Farnoux, J. Phys. (Paris) 40, 545 (1979).
[6]A. F. Starace and L. Armstrong, Jr., Phys. Rev. A 13, 1850 (1976).
[7]N. A. Cherpkov and L. V. Chernysheva, Phys. Lett. 60A, 103 (1977).
[8]K. Kimura, T. Yamazaki, and Y. Achiba, Chem. Phys. Lett. 58, 104 (1978).
[9]M. J. Conneely, Ph.D. thesis, London University, 1969 (unpublished).
[10]S. T. Manson, A. Msezane, A. F. Starace, and S. Shahabi, Phys. Rev. A 20, 1005 (1979).
[11]H. P. Kelly, Adv. Theor. Phys. 2, 75 (1968); Adv. Chem. Phys. 14, 129 (1969).
[12]S. L. Carter and H. P. Kelly, Phys. Rev. A 13, 1388 (1976).
[13]U. Fano and J. W. Cooper, Rev. Mod. Phys. 40, 441 (1968).
[14]H. P. Kelly and A. Ron, Phys. Rev. A 5, 168 (1972).
[15]R. L. Chase and H. P. Kelly, Phys. Rev. A 6, 2150 (1972).
[16]M. Ya. Amus'ya, N. A. Cherepkov, and L. V. Chernysheva, Zh. Eksp. Teor. Fiz. 60, 160 (1971) [Sov. JETP 33, 90 (1971)].
[17]R. M. Sternheimer, Phys. Rev. 115, 1198 (1959).
[18]H. Kelly and R. Simons, Phys. Rev. Lett. 30, 529 (1973).
[19]L. M. Frantz, R. L. Mills, R. G. Newton, and A. M. Sessler, Phys. Rev. Lett. 1, 340 (1958); B. A. Lippmann, M. H. Mittleman, and K. M. Watson, Phys. Rev. 116, 920 (1959); R. T. Pu and E. S. Chang, *ibid.* 151, 31 (1966); H. J. Silverstone and M. L. Yin, J. Chem. Phys. 49, 2026 (1968); S. Huzinaga and C. Arnau, Phys. Rev. A 1, 1285 (1970).
[20]C. E. Moore, *Atomic Energy Levels*, U. S. Natl. Bur. Stand. Circ. No. 467 (U. S. GPO, Washington, D. C., 1949).
[21]A. W. Fliflet and H. P. Kelly, Phys. Rev. A 10, 508 (1974).
[22]A. F. Starace, in *Handbach der Physik*, Vol. 31 (to be published).
[23]M. J. Seaton, Philos. Trans. R. Soc. London A 245, 469 (1953); K. Smith, R. J. W. Henry, and P. G. Burke, Phys. Rev. 147, 21 (1966).
[24]A. E. Hansen, Mol. Phys. 13, 425 (1967).
[25]R. D. Cowan, L. J. Radziemski, Jr., and V. Kaufman, J. Opt. Soc. Am. 64, 1474 (1974).
[26]M. Pindzola and H. Kelly, Phys. Rev. A 12, 1419 (1975).
[27]M. Ya. Amus'ya in *Invited Papers and Progress Reports, Eighth International Conference on the Physics of Electronic and Atomic Collisions, Belgrade, 1973,* edited by B. C. Čorbić and M. V. Kurepa (Institute of Physics, Belgrade, 1973), p. 171.
[28]P. G. Burke and K. T. Taylor, J. Phys. B 8, 2620 (1975).
[29]J. A. R. Samson and J. L. Gardner, Phys. Rev. Lett. 33, 671 (1974).
[30]L. Armstrong, Jr., and W. R. Fielder, Phys. Scr. (to be published).
[31]J. R. Swanson and L. Armstrong, Jr., Phys. Rev. A 16, 1117 (1977).
[32]J. Berkowitz and G. L. Goodman, J. Chem. Phys. 71, 1754 (1979).
[33]J. Berkowitz (private communication).